Journal of Applied Polymer Science

Numerical investigation of spinneret geometric effect on spinning dynamics of dry-jet wet-spinning of cellulose/[BMIM]Cl solution

Xiaolin Xia, Jianning Wang, Huaping Wang, Yumei Zhang
State Key Laboratory for Modification of Chemical Fibers and Polymer Materials, College of Materials Science and Engineering, Donghua University, Shanghai 201620, China
Correspondence to: Y. Zhang (E-mail: zhangym@dhu.edu.cn)

ABSTRACT: In this study, the effect of spinneret geometry, including the entrance angle α of the entrance channel, the length L_s, and the diameter D_0 of the exit channel, on the spinning dynamics of dry-jet wet-spinning of cellulose/1-butyl-3-methylimidazolium chloride ([BMIM]Cl) solution was simulated by using finite element method. Based on the mathematical model of dry-jet wet-spinning established in our previous work (Xia *et al.*, *Cellulose* 2015, 22, 1963) the radial and axial profiles of velocity, pressure, and shear rate in the spinneret and the profiles of diameter, temperature, and tensile stress in the air-gap region were obtained. From the simulated profiles, the effect of spinneret geometric parameters on the flow behavior and the pressure drop of polymer solution in the spinneret and the die-swell ratio near the spinneret was discussed. The entrance angle α of the entrance channel mainly influences the flow behavior of polymer solution in the spinneret and the die-swell effect near the spinneret. As the decrease of the entrance angle α of the entrance channel, the vortices in the spinneret could be removed and the die-swell ratio decreases. The increase of the length L_s of the exit channel results in the increase of pressure drop in the spinneret and the decrease of the die-swell ratio. It is also found that the increase of the diameter D_0 of the exit channel reduces the flow velocity of polymer solution and decreases the pressure drop in the spinneret at a constant mass flow rate. © 2016 Wiley Periodicals, Inc. J. Appl. Polym. Sci. **2016**, *133*, 43962.

KEYWORDS: cellulose and other wood products; fibers; ionic liquids; theory and modeling; viscosity and viscoelasticity

Received 7 January 2016; accepted 22 May 2016
DOI: 10.1002/app.43962

INTRODUCTION

Using direct solvents such as *N*-methylmorpholine-*N*-oxide[1–3] and ionic liquids[4,5] to produce regenerated cellulose fibers is an alternative to the viscose-technology. For such nonderivative technology, although both wet-spinning[5,6] and dry-jet wet-spinning[7–9] routes were reported, the later route is commonly applied in the industry-scale process. The essential difference between wet-spinning and dry-jet wet-spinning routes could be summarized into two points. One is that an elongational flow is added into the air-gap region in which the extruded solutions are precooled and even translated into gels. Meanwhile, the polymer chains are stretched and oriented at a certain tensile stress before fibers enter into the coagulation bath during dry-jet wet-spinning process.[10,11] The effect of air-gap conditions on the fibers during dry-jet wet-spinning process has been investigated for various polymer solutions.[8–11] In fact, the other difference between wet-spinning and dry-jet wet-spinning is the spinneret. The length of the spinneret for wet-spinning is short and the shear flow of the concentrated solution during the spinneret could be ignored while the length of spinneret for dry-jet wet-spinning is usually longer which is similar to that of the melt spinning, in which the shear flow of the concentrated solution must be considered.

From the bits and pieces of information, the effect of spinneret geometry on the spinning technology and structure of fiber could be seen obviously.[12–17] Kirichenko *et al.*[12] reported that the effect of spinneret geometry on the regularity of the properties of Capron cord yarn. It was found that in the case of yarns spun through circular spinnerets the irregularity of the diameter and birefringence is greater than that for yarns spun through rectangular spinnerets. A test of the effect of spinneret hole length on fiber diameter was carried out by Bostwick[13] and it was found that the long holes extruded less materials than the short holes for a homogeneous polymer solution. Wang *et al.*[16] studied the effects of flow angle and shear rate within the spinneret on the separation performance of poly(ethersulfone) ultrafiltration hollow fiber. The results showed that the flow angle in the spinneret provides another variable in controlling the pure water permeability, solute separation, pore size, and pore size distribution of hollow fibers. Also, Chen *et al.*[17] investigated that the port angle of the spinneret had a significant influence on the character of the resultant Janus nanofibers. By

manipulating this parameter, Janus nanofiber with tunable structures in terms of width, interfacial area, and also volume of each side can be fabricated. From above discussions, although we get the point that spinneret geometry affects structure and properties of fibers greatly, how the way changes or what is happened in the spinneret is still an issue. It is not easy for us to conquer this issue by experiments as the dimension of the spinneret is pretty tiny and the manufacturing process of the spinneret is complicated.

As the development of computer technology, simulation is used as a powerful tool to solve some issues which are not easy to be measured by experiments, and directly has been widely used in scientific and industrial fields. Some considerable effects also have been done by some researchers.[18–22] Zhou *et al.*[18] proposed the optimum spinning condition for the desired noncircular fiber based on the numerical experiments and the optimum spinning condition was well validated by experiments. The numerical simulation could be very efficient in the design and process of shaped fibers. In our past work,[21] the effect of spinneret geometry on flow behavior of spinning dope in the spinneret was reported. However, only an isothermal model was adopted to simulate the flow behavior in the spinneret and some important spinning parameters were ignored, such as air-gap lengths, draw velocity, surrounding temperature, and humidity. Afterwards, a compressive model[22] was established to disclose the dynamics of dry-jet wet-spinning, in which the effect of viscoelasticity of polymer solution, flow behavior in the spinneret, and nonisothermal effect in the air-gap region was considered.

Continued with our previous work, the effect of the geometric parameters of the spinneret on the dynamics of dry-jet wet-spinning of cellulose/[BMIM]Cl solution was investigated by numerical simulation in this work. As the spinneret parameters including the entrance angle α of the entrance channel, the length L_s, and the diameter D_0 of the exit channel varied, the profiles of velocity, pressure, and shear rate in the spinneret and profiles of velocity, diameter, temperature, and tensile stress in the air-gap region were obtained and then flow behavior, pressure drop, and die-swell ratio were discussed further.

MATHEMATICAL FORMULATION

Description of Dry-Jet Wet Spinning Process

In dry-jet wet-spinning process, as shown in Figure 1, a polymer filament is extruded from a spinneret into an air-gap region at a mass flow rate W and temperature T_i. The filament is then elongated at an ambient temperature T_{amb} by a take-up device with a take-up speed V_1. The filament cools as it passes through the air-gap region with a specific length L, and orientation begins to occur at a certain take-up force. There is a reduction in diameter of the filament in the air-gap region at a certain take-up speed V_1. However, after the filament reaches a distance, the value of filament diameter could not have an obvious reduction and roughly equals to the value on the first roller if we neglect the diffusion process in the coagulation bath. In this case, we think the filament has already reached complete deformation before entering the coagulation bath. Therefore, the correlation of $V_d = V_1$ is obtained and we will focus on this situation in the current work. In addition, in order to study the spinneret geometric effect on dynamics of dry-jet wet-spinning, the fluid flow will be discussed in the domain $Z_0 \leq Z \leq Z_2$, shown in Figure 1.

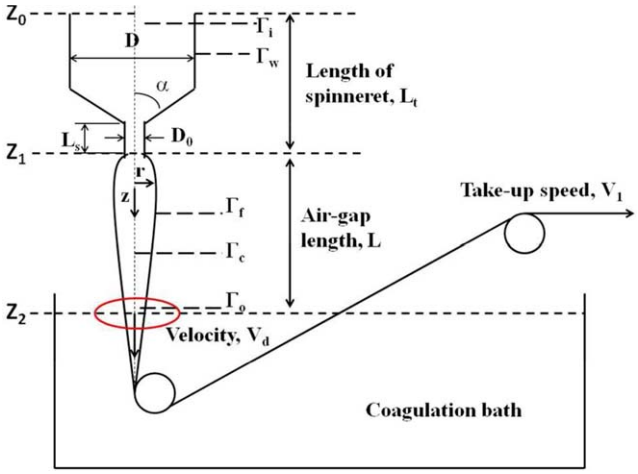

Figure 1. Schematic illustration of forming process of the dry-jet wet-spinning process (D is the diameter of entrance channel, D_0 is the diameter of exit channel, L_s is the length of exit channel, α is the entrance angle, other parameters in this figure will be discussed in detail in the article). [Color figure can be viewed in the online issue, which is available at wileyonlinelibrary.com.]

Governing Equation

In dry-jet wet-spinning process, the flow under consideration is in the steady state and nonisothermal viscoelastic flow without phase transition encountered in the air-gap region. It is assumed that the flow direction is vertically downward and the flow field is axisymmetric. A cylindrical coordinate system is used, as shown in Figure 1.

Continuity Equation. Cellulose/[BMIM]Cl solution is assumed as an incompressible viscoelastic fluid and the cooling medium is atmospheric dry air. Neglecting the mass transfer process between fluid and cooling medium, the continuity equation can be written as eq. (1).

$$\nabla \cdot \boldsymbol{\upsilon} = 0 \tag{1}$$

where υ is the velocity vector.

Momentum Equation. Surface tension and air friction have a little effect on the force balance equation due to the large viscosity of cellulose/[BMIM]Cl solution.[23,24] Therefore, the momentum equation can be written as eq. (2).

$$\rho\left(\frac{\partial \boldsymbol{\upsilon}}{\partial t} + \boldsymbol{\upsilon} \cdot \nabla \boldsymbol{\upsilon}\right) = \rho \boldsymbol{g} + \nabla \cdot \boldsymbol{\tau} - \nabla p \tag{2}$$

where ρ is the density of fluid (for polymer and solvent system, ρ is a function of concentration and temperature); $\boldsymbol{g}$ is gravity acceleration (9.8 m/s^2); p is the hydrostatic pressure; τ is the total extra stress tensor; $\boldsymbol{D}$ is the rate-of-deformation tensor.

$$\boldsymbol{D} = \frac{(\nabla \boldsymbol{\upsilon} + \nabla \boldsymbol{\upsilon}^T)}{2} \tag{3}$$

Energy Equation. Neglecting the heat conduction along the axial direction of the fluid, only the heat transfer process

between cooling medium and fluid is taken into consideration. Therefore, the energy equation can be written as eq. (4).

$$\rho C_p \frac{dT}{dt} = -\nabla \cdot \boldsymbol{q} + \boldsymbol{\tau} : \nabla \boldsymbol{v} \quad (4)$$

where C_p is the heat capacity (for polymer and solvent system, C_p is a function of concentration and temperature); $\boldsymbol{q}$ is the heat flux.

Constitutive Equation. The constitutive equation is an equation which can be used to describe the viscoelastic flow of polymer melts or solutions. According to our previous study,[22] an exponential PTT model captures the viscoelastic rheological properties of cellulose/[BMIM]Cl solution properly, which takes the following form:

$$\exp\left[\frac{\varepsilon\lambda}{\eta}\mathrm{tr}(\boldsymbol{\tau})\right]\boldsymbol{\tau} + \lambda\left[\left(1-\frac{\xi}{2}\right)\overset{\nabla}{\boldsymbol{\tau}} + \frac{\xi}{2}\overset{\Delta}{\boldsymbol{\tau}}\right] = 2\eta\boldsymbol{D} \quad (5)$$

where

$$\overset{\nabla}{\boldsymbol{\tau}} = \boldsymbol{v}\cdot\nabla\boldsymbol{\tau} - \nabla\boldsymbol{v}^{\mathrm{T}}\cdot\boldsymbol{\tau} - \boldsymbol{\tau}\cdot\nabla\boldsymbol{v} \quad (6)$$

and

$$\overset{\Delta}{\boldsymbol{\tau}} = \boldsymbol{v}\cdot\nabla\boldsymbol{\tau} + \boldsymbol{\tau}\cdot\nabla\boldsymbol{v}^{\mathrm{T}} + \nabla\boldsymbol{v}\cdot\boldsymbol{\tau} \quad (7)$$

are, for steady state, the Upper-Convected and Lower-Convected derivative of the total extra stress tensor τ, respectively; λ is the relaxation time. ε and ξ are two important model parameters. ϵ is elongational parameter, which has a strong influence on the elongational behavior of the material. ξ is mobility factor, which is related to the slip between the molecular network and the continuum medium. The characteristic feature is that PTT model incorporates memory effect of material, which is able to describe the viscoelasticity of polymer solution perfectly.

The effect of the temperature on the viscoelasticity of polymer solution complies with time–temperature superposition. Therefore, the relaxation time λ and viscosity η can be expressed as[25]:

$$\lambda(T) = \alpha_T\lambda(T_0) \quad (8)$$

$$\eta(T) = \alpha_T\eta_0(T_0) \quad (9)$$

where T is the absolute temperature of polymer solution; T_0 is the reference temperature of polymer solution; α_T is shift factor, which can be obtained from the Arrhenius equation.

$$\ln(\alpha_T) = \ln\left(\frac{\eta}{\eta_0}\right) = \left[\frac{\Delta H}{R}\left(\frac{1}{T}-\frac{1}{T_0}\right)\right] \quad (10)$$

In which ΔH is the flow activation energy, which can be calculated from shear viscosity data at various temperatures using the Arrhenius equation. R (=8.314 J K^{-1} mol^{-1}) is the gas constant.

Boundary Conditions

Let Γ_i, Γ_w, Γ_f, Γ_c, and Γ_o denote the inflow, wall, free face, centerline, and outlet boundaries, respectively. The boundary conditions for the dry-jet wet-spinning process under consideration may be written as

$$\Gamma_i : \upsilon = \upsilon(r), \tau = \tau(r) \text{ and } T = T_i \quad (11)$$

$$\Gamma_w : \upsilon = 0 \text{ and } T = T_w \quad (12)$$

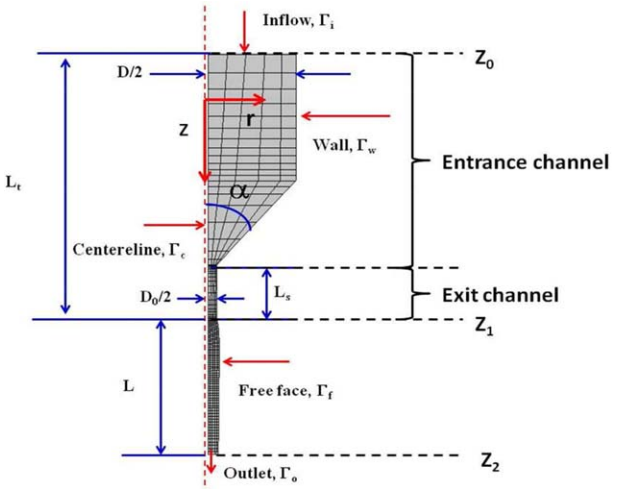

Figure 2. Two-dimensional spinning model and finite element meshes. [Color figure can be viewed in the online issue, which is available at wileyonlinelibrary.com.]

$$\Gamma_c : \upsilon_r = 0, \tau : nt = 0 \text{ and } q\cdot n = 0 \quad (13)$$

$$\Gamma_o : \upsilon_z = V_1, F_r = 0 \text{ and } q\cdot n = 0 \quad (14)$$

where T_i is the temperature on inflow boundary, T_w is the temperature on wall, $\boldsymbol{n}$ and $\boldsymbol{t}$ are the outward normal and tangent unit vectors to the boundary, $\boldsymbol{q}$ is the thermal flux, V_1 is take-up speed, F_r is the traction force in radial direction.

The free face conditions can be described as:

$$\Gamma_f : \tau\cdot n = 0, \upsilon\cdot n = 0 \text{ and } q\cdot n = h(T - T_{\mathrm{amb}}) \quad (15)$$

where h is the heat transfer coefficient, which is related to material properties and specific process.

NUMERICAL METHOD

The spinneret is composed of an entrance channel and an exit channel, shown in Figure 2. In this study, spinnerets with various entrance channels and exit channels are designed to investigate the effect of spinneret geometry on the spinning dynamics. There are three geometric parameters of spinneret we discussed, including the entrance angle α of the entrance channel, the length L_s and the diameter D_0 of the exit channel. In addition, the diameter D of the entrance channel and the length of the spinneret L_t is assumed as 2 mm and 3.6 mm, respectively. The length L of air-gap region we adopted is 180 mm. The reason why we employed this value is based on experimental data discussed in our previous work.[22]

Simulations are performed by using POLYFLOW software (version 14.5), which is a finite-element computational fluid dynamics software. Figure 2 is the two-dimensional spinning model and finite element meshing. Because a large velocity gradient generally occurs near the die exit, finer meshes are divided near the die outlet and sparser meshes are adopted in the direction away from the die with the successive ratio of 1.02. Within each element the velocity and temperature component are approximated by using quadratic interpolation function, the pressure by a linear function, while the stress is approximated by an Elastic-Viscous Splitting of the Stress/Streamline-Upwind

Table I. Physical and Rheological Parameters of 6 wt % Cellulose/[BMIM]Cl Solution Used in the Simulations

Properties	Parameters
Density, ρ (kg/m^3)	$\rho = 1234.9\text{-}0.505\ T$
Heat capacity, C_p (kJ/kg·K)	$C_p = 1331.7 + 2.743\ T$
Heat transfer coefficient, h (W/m^2·K)	$h = k\cdot(v/S)^n$, k·=9.81, n=0.24
Flow activation energy, ΔH (kJ/mol)	60.8
Zero shear viscosity at 353 K, η_0 (Pa s)	196.8
Relaxation time at 353K, λ (s)	0.35
Elongational parameter, ϵ	0.03
Mobility factor, ξ	0.02

Table II. Processing Parameters for Dry-Jet Wet-Spinning of 6 wt % Cellulose/[BMIM]Cl Solution Used in the Simulations

Processing parameter	Value
Diameter of entrance channel, D (mm)	2
Diameter of exit channel, D_0 (mm)	0.15, 0.20, 0.30, 0.60
Length of exit channel, L_s (mm)	0.20, 0.40, 0.60, 0.80
Entrance angle, α (°)	30, 45, 60, 90
Mass flow rate, W (g/min)	0.1236
Spinning temperature, T_i (K)	353
Ambient temperature, T_{amb} (K)	293
Take-up speed, V_1 (m/s)	0.12
Air-gap length, L (mm)	180

(EVSS SU) form. EVSS is a technique of finite element methods where the extra stress tensor is split into purely elastic and viscous components. SU integration of the governing equation coupled with finite element treatment of equation of motion and continuity extends the limit of convergence of the numerical method. Therefore, the combination between EVSS and SU produce a stable and accurate discretization for flow of viscoelastic fluids in smooth geometries. The numerical convergence criterion is 10^{-6}.

INPUT PARAMETERS

The simulations were performed on 6 wt % cellulose/[BMIM]Cl solution in this study. The polymerization degree of cellulose was 505 and [BMIM]Cl was synthesized and purified in our

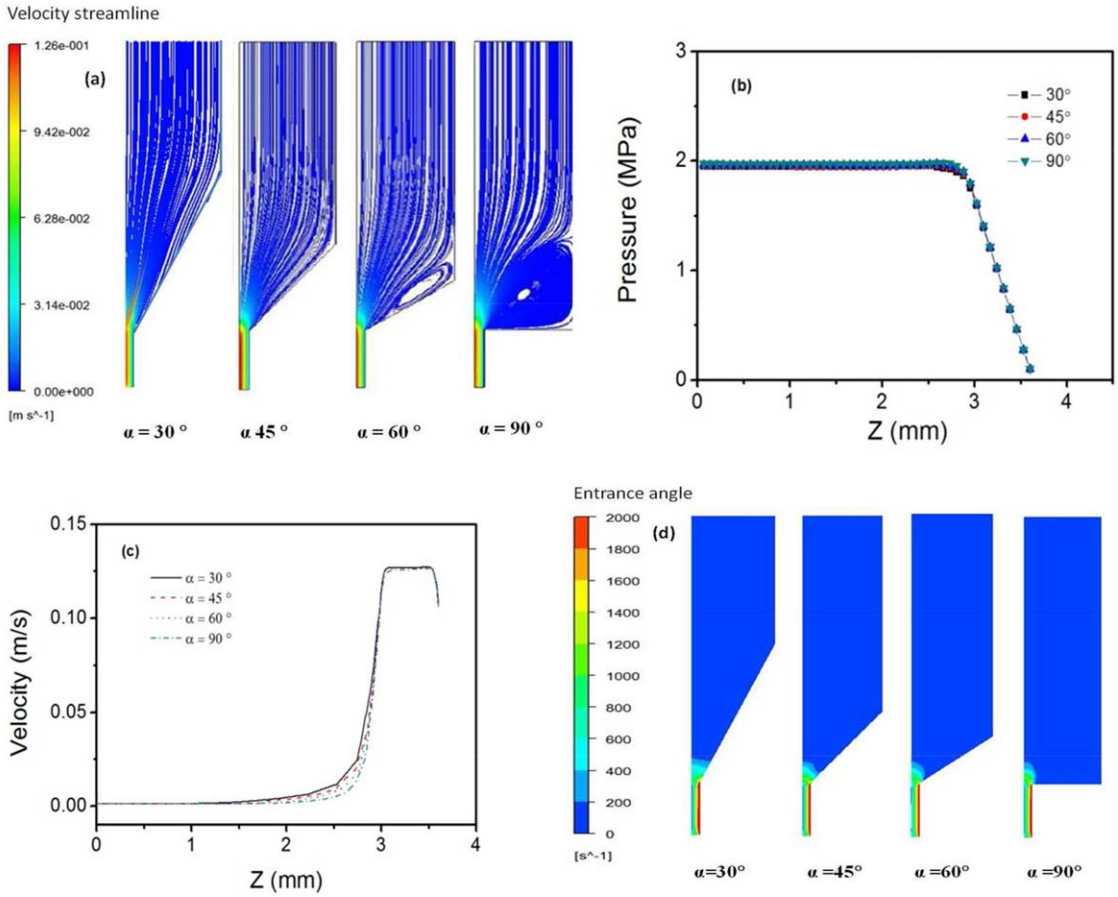

Figure 3. The profiles of (a) velocity streamline, (b) pressure, (c) velocity, (d) shear rate, in the spinneret ($Z_0 \le Z \le Z_1$) with various entrance angles α of exit channel. [Color figure can be viewed in the online issue, which is available at wileyonlinelibrary.com.]

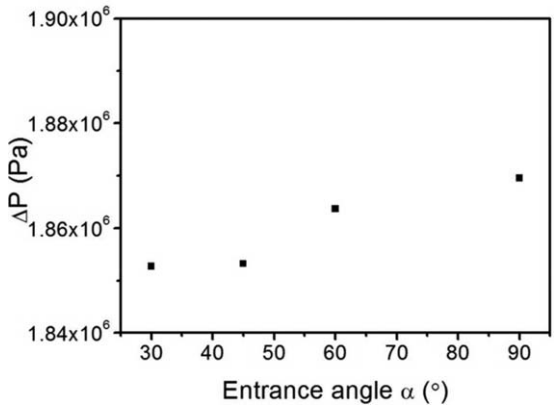

Figure 4. Comparison of overall pressure drop ΔP at different entrance angles α of entrance channel.

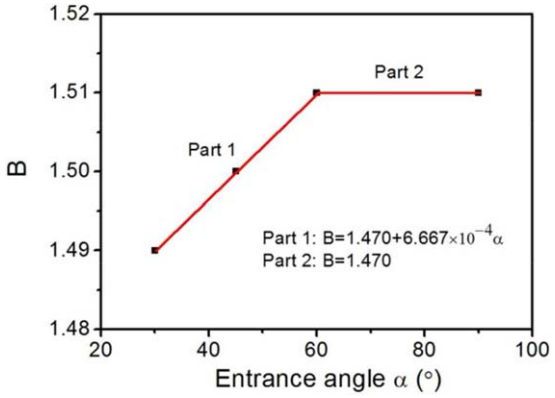

Figure 6. Comparison of die-swell ratio B at different entrance angles α of entrance channel. [Color figure can be viewed in the online issue, which is available at wileyonlinelibrary.com.]

laboratory. The water content of [BMIM]Cl measured by the Karl Fisher titration (ZSD-2 Shanghai Anting Electric Instruments Co. Ltd., China) is less than 0.1 wt % with a precision of 0.05%. The physical and rheological parameters of 6 wt % cellulose/[BMIM]Cl solution are summarized in Table I, which corresponding to the material parameters in the simulations. These parameters were reported in our previous study,[22] so the data was cited directly in this work. The processing parameters are summarized in Table II.

RESULTS AND DISCUSSION

The entrance angle α of entrance channel, the length L_s and the diameter D_0 of the exit channel are the key parameters for the designing and processing of the spinneret. Meanwhile, the effect of the above parameters on the fiber formation could not be neglected. As the effect of the spinneret parameters on the spinning results is difficult to be measured by experiments, the dynamics of dry-jet wet-spinning of cellulose/[BMIM]Cl solution with various spinneret parameters was investigated by the model we established above. The radial and axial profiles of velocity, pressure, diameter, temperature, and stress along the spinning line from the inlet of the spinneret to the end of the air-gap region will be discussed in detail to illustrate the effect of the spinneret parameters on flow behavior, the pressure drop, and die-swell ratio of the polymer solutions.

During the dry-jet wet-spinning process shown in Figure 1, the flow of polymer solution consists of two processes, one process is

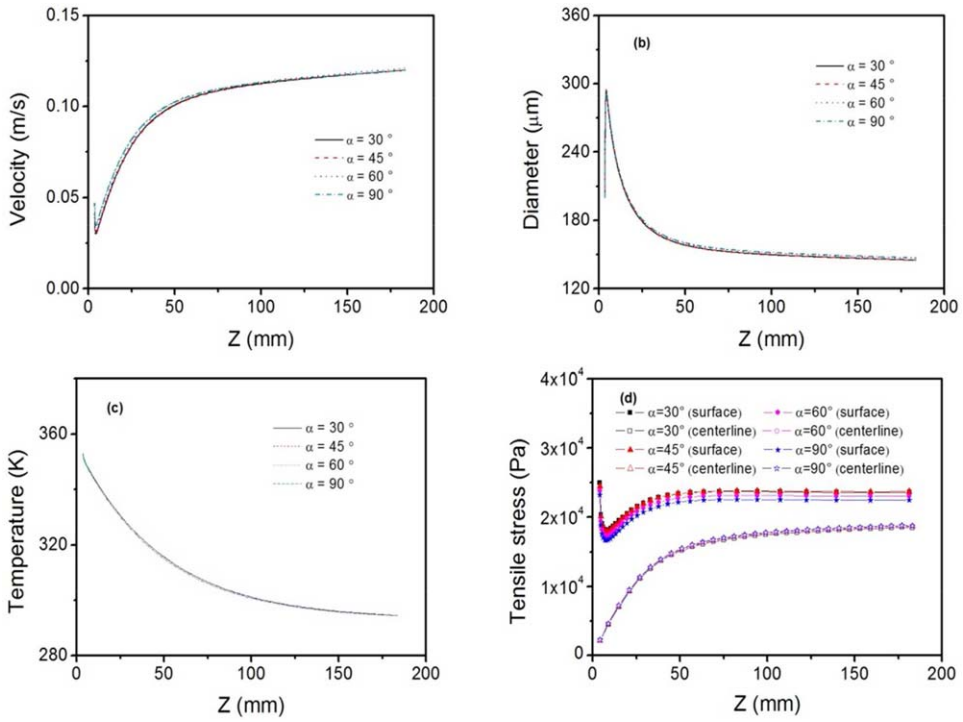

Figure 5. The profiles of (a) velocity, (b) diameter, (c) temperature, (d) tensile stress, in the air-gap region ($Z_1 \leq Z \leq Z_2$) for the solution extruded from the spinneret with various entrance angles α. [Color figure can be viewed in the online issue, which is available at wileyonlinelibrary.com.]

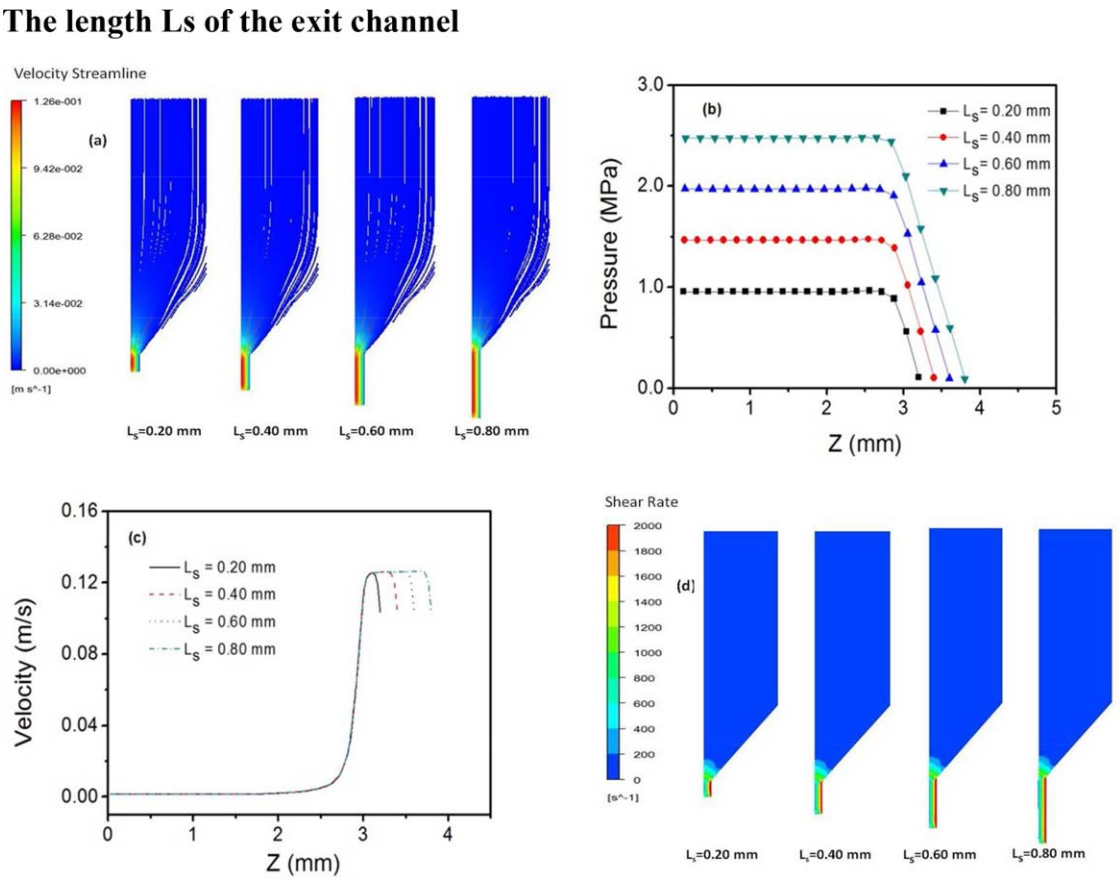

Figure 7. The profiles of (a) velocity streamline, (b) pressure, (c) velocity, (d) shear rate, in the spinneret ($Z_0 \leq Z \leq Z_1$) with various lengths L_s of exit channel. [Color figure can be viewed in the online issue, which is available at wileyonlinelibrary.com.]

the contraction flow in the spinneret and the other is the elongational flow in the air-gap region. Therefore, we will discuss the effect of spinneret geometric parameters on the spinning dynamics starting from the flow behaviors in the spinneret.

The Entrance Angle α of the Entrance Channel

In this section, a variable entrance angle α of the entrance channel with definite $L_s = 0.60$ mm and $D_0 = 0.20$ mm is firstly employed. The input parameters and the boundary conditions are consistent with we discussed above.

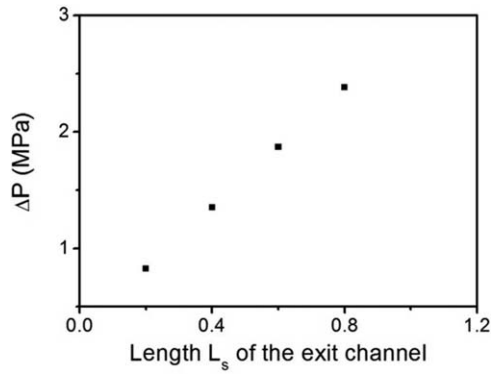

Figure 8. Comparison of overall pressure drop ΔP at different lengths L_s of exit channel.

The comparison of profiles of velocity streamline, pressure, velocity, and shear rate in the spinneret with different entrance angles α of the entrance channel under definite $L_s = 0.60$ mm and $D_0 = 0.20$ mm is shown in Figure 3. It is found that the entrance angles α has little effect on the profiles of pressure, velocity, and shear rate in the spinneret. However, there are vortices existing in the corner of the spinneret and the size of these vortices decreases with the decrease of entrance angles α of the entrance channel, shown in Figure 3(a). These vortices can lead to "dead" region, which increase the residence time of fluids in the spinneret and reduce the efficiency of transportation. Fortunately, the vortices are completely removed when the entrance angle $\alpha = 45°$, which suggests that the fluids can flow steadily in the spinneret. It is reported that the formation of vortices not only relates to the rheological properties of polymer solution,[26,27] but also correlates the geometry of flow channel.[28,29] Therefore, it is a direct and effective way to eliminate the vortices by decreasing the entrance angle α of the entrance channel.[30–32] In addition, the variation of entrance angles α has little effect on the overall pressure drop ΔP in the spinneret, which is defined as the pressure drop for flowing from the start area to goal area, shown in Figure 4.

Figure 5 shows the comparison of profiles of velocity, diameter, temperature, and tensile stress in the air-gap region for the solution extruded from the spinneret with different entrance

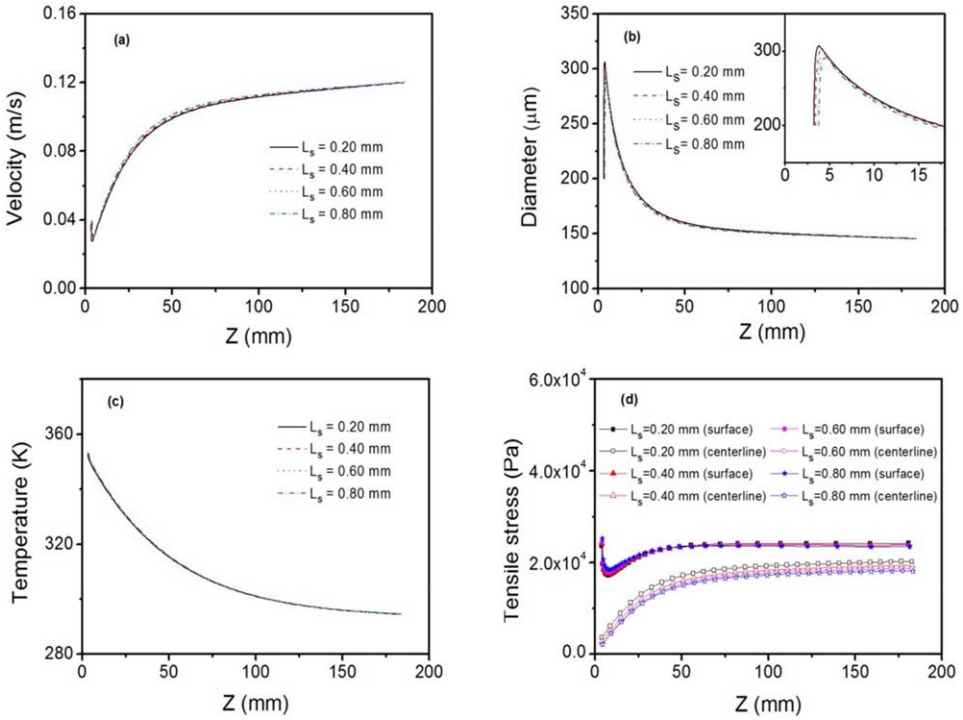

Figure 9. The profiles of (a) velocitiy, (b) diameter, (c) temperature, (d) tensile stress, in the air-gap region ($Z_1 \leq Z \leq Z_2$) for the solution extruded from the spinneret with various lengths L_s of exit channel. [Color figure can be viewed in the online issue, which is available at wileyonlinelibrary.com.]

angles α of the entrance channel under definite $L_s = 0.60$ mm and $D_0 = 0.20$ mm. It can be found that there is little change of velocity, diameter, temperature, and tensile stress in the air-gap region as the variation of entrance angle α. However, the variation of entrance angle α of the entrance channel influences the die-swell ratio B, which is defined as $B = D_{max}/D_0$. Here, D_{max} is the maximal value of diameter; D_0 is the diameter of the exit channel, shown in Figure 6. As shown in Figure 6, the dependence of entrance angle α on die-swell ration B could be divided into two parts. The part 1 shows that the die-swell ratio B increases with the increase of entrance angle α in the range from 30° to 60° and could be concluded as following equation: $B = 1.470 + 6.667 \times 10^{-4}\alpha$. During the part 2, as the entrance angle α increases, there is no significant variation in die-swell ratio B. The equation could be expressed as $B = 1.470$. It also indicates that elastic deformation could reach the maximal value at a certain entrance angle α. For this phenomena, it could be attributed to the extending of the flowing length, which makes the polymer chains have more sufficient time to relax, as well as the reduction of the velocity gradient along the flow direction with the decrease of the entrance angle α.

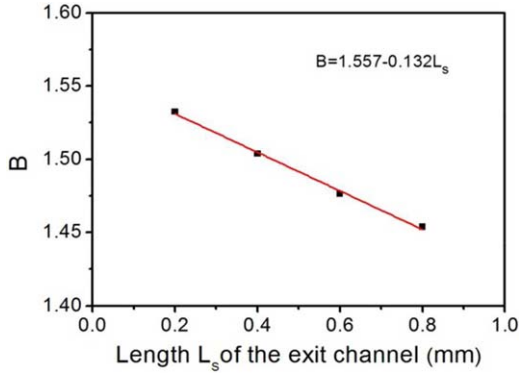

Figure 10. Comparison of die-swell ratio B at different lengths L_s of exit channel. [Color figure can be viewed in the online issue, which is available at wileyonlinelibrary.com.]

The Length L_s of the Exit Channel

Next, the effect of the length L_s of the exit channel on the dynamics of dry-jet wet-spinning of cellulose/[BMIM]Cl solution will be discussed. Here, the entrance angle α of the entrance channel and the diameter D_0 of the exit channel are fixed at 45° and 0.20 mm, respectively. The input parameters and the boundary conditions are consistent with we discussed above.

Figure 7 shows the comparison of profiles of velocity streamline, pressure, velocity, and shear rate in the spinneret with different lengths L_s of the exit channel under definite $D_0 = 0.20$ mm and $\alpha = 45°$. It can be found that the variation of the length L_s of the exit channel has little effect on the profiles of velocity streamline, velocity, and shear rate. As fluid elements approach the contraction, they begin to converge into trickle and flow more rapidly into the downtown, shown in Figure 7(a). This tapering effectively reduces the cross-sectional area of flow and contributes to the pressure drop, shown in Figure 7(b). In order to show the variation of velocity in the spinneret clearly, the data along the centerline was extracted and plotted in Figure 7(c). From the initial stage of the spinning line, there is no increase in the velocity and an abrupt increase of velocity was observed at a location approximately 2.5 mm. The velocity

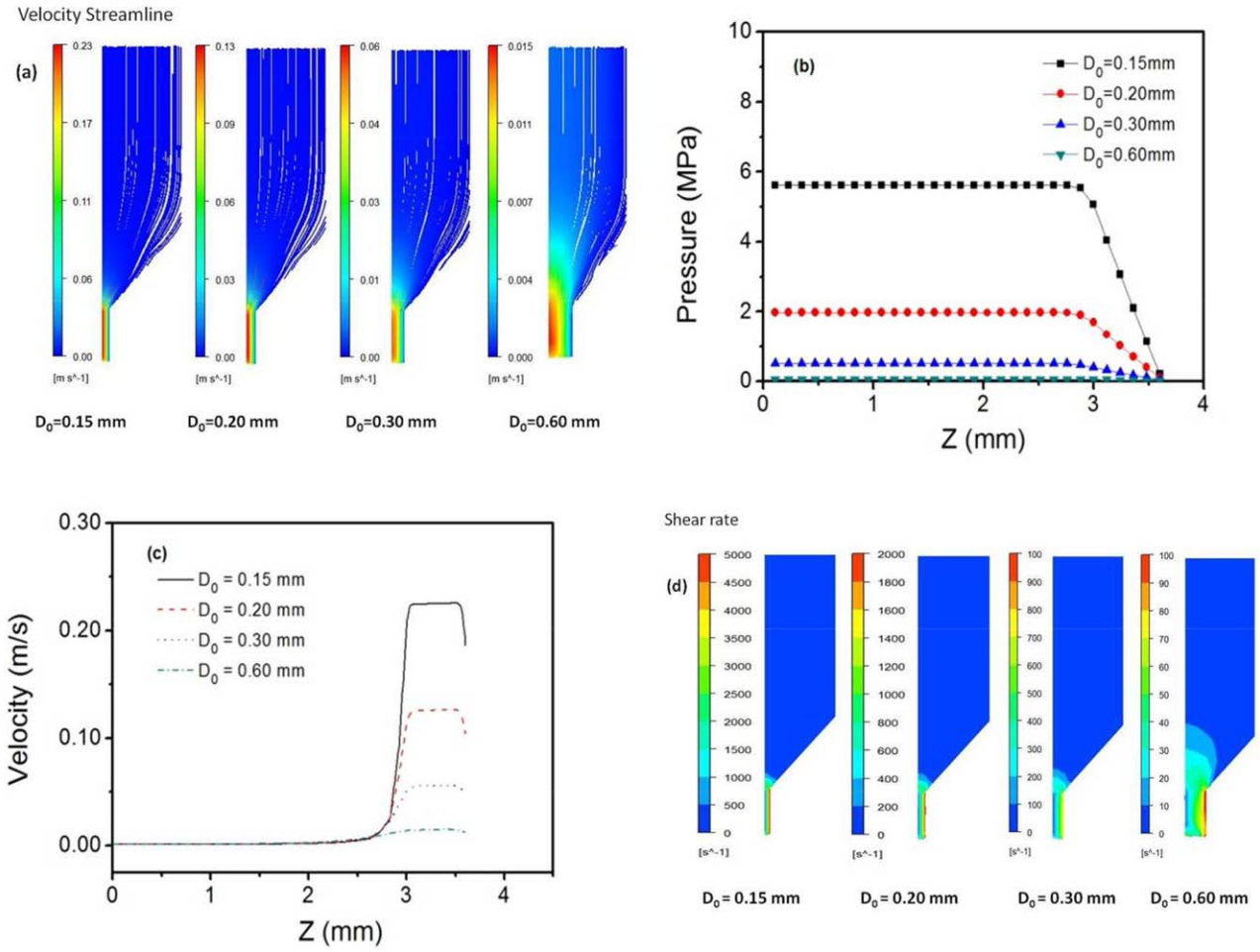

Figure 11. The profiles of (a) velocity streamline, (b) pressure, (c) velocity, (d) shear rate, in the spinneret ($Z_0 \leq Z \leq Z_1$) with various diameters D_0 of exit channel. [Color figure can be viewed in the online issue, which is available at wileyonlinelibrary.com.]

starts to increase dramatically in the vicinity of the contraction area.

As shown in Figure 7(b), the pressure in the spinneret varies greatly with the length L_s of the exit channel. It can be found that the pressure keeps increasing with the increase of the length L_s, but the shape of pressure profile along the flow path are similar to each other. For each pressure profile, there is almost no decay in the pressure in the initial region. The pressure begins to decrease linearly when the solution is flowing in the vicinity of the contraction. The presence of an abrupt contraction during pressure driven flow of polymer solution gives rise to an additional pressure drop associated with relevant storage and viscous dissipation of the deformation energy.[33] In order to estimate the dissipated energy in the spinneret, overall pressure drop ΔP is employed, shown in Figure 8. It can be found that the overall pressure drop ΔP increases linearly with the increase of length L_s of the exit channel, which suggests that it is easier for longer channel to dissipate energy in the spinneret.

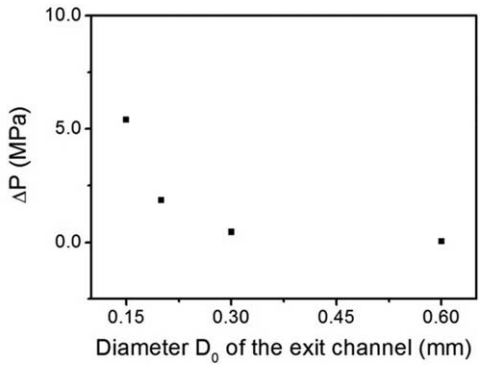

Figure 12. Comparison of overall pressure drop ΔP at different diameters D_0 of exit channel.

Figure 9 shows the comparison of profiles of velocity, diameter, temperature, and tensile stress in the air-gap region for the solution extruded from the spinneret with different lengths L_s of the exit channel under definite $D_0 = 0.20$ mm and $\alpha = 45°$. Obviously, the variation of the length L_s of the exit channel has little effect on the profiles of velocity, diameter, temperature, and tensile stress. As shown in Figure 9(a), there is a reduction in velocity profile in the region close to the spinneret, which corresponds to the die-swell phenomena in diameter profile shown in Figure 9(b). When the polymer solution is flowing

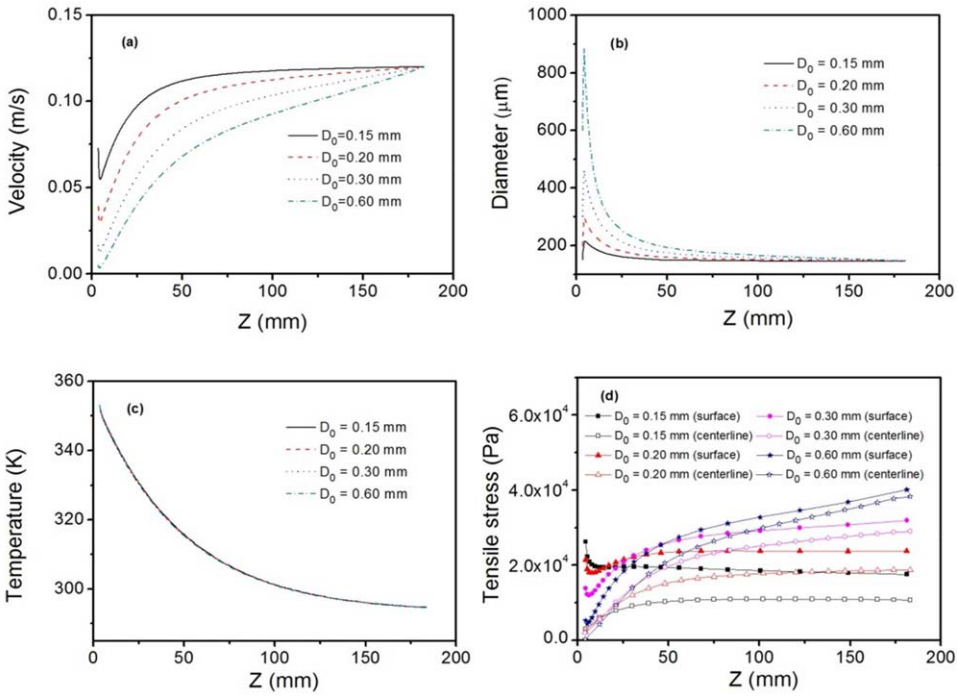

Figure 13. The profiles of (a) velocity, (b) diameter, (c) temperature, (d) tensile stress, in the air-gap region ($Z_1 \leq Z \leq Z_2$) for the solution extruded from the spinneret with various diameters D_0 of exit channel. [Color figure can be viewed in the online issue, which is available at wileyonlinelibrary.com.]

through the spinneret, there is a mix of shear and extensional deformation. Therefore, most of energies are stored in the form of elastic deformation. When the fluids are extruded from the exit channel, elastic deformation recovers and die-swell effect occurs. Figure 10 shows the comparison of die-swell ratio B at different lengths L_s of the exit channel. As shown in Figure 10, the die-swell ratio B decreases linearly with the increase of the length L_s of exit channel and could be concluded as following equation: $B = 1.557 - 0.132L_s$. It is found that the die-swell ratio B decreases from 1.533 to 1.454 with the length L_s of the exit channel increasing from 0.20 mm to 0.80 mm. It means that the increase of the length L_s of the exit channel can help to reduce the die-swell effect in the polymer processing, which is attributed to the relaxation of polymer chains.[34,35]

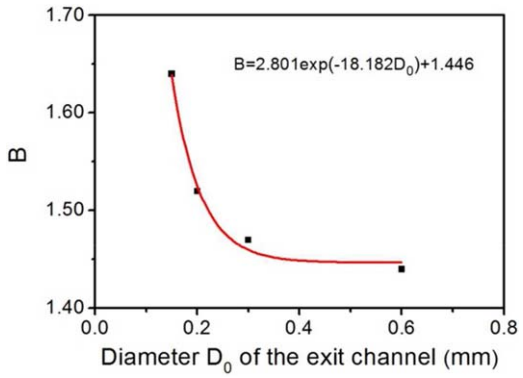

Figure 14. Comparison of die-swell ratio B at different diameters D_0 of exit channel. [Color figure can be viewed in the online issue, which is available at wileyonlinelibrary.com.]

The Diameter D_0 of the Exit Channel

Beside the length L_s of the exit channel, the diameter D_0 of the exit channel is another important parameter for the spinneret. In this section, we will discuss the effect of the diameter D_0 of the exit channel on the dynamics of dry-jet wet-spinning of cellulose/[BMIM]Cl solution. The length L_s of the exit channel and the entrance angle α of the entrance channel are fixed at 0.60 mm and 45°, respectively. The input parameters and the boundary conditions are consistent with we discussed above.

Figure 11 shows the comparison of profiles of velocity streamline, pressure, velocity, and shear rate in the spinneret with different diameters D_0 of the exit channel under definite $L_s = 0.60$ mm and $\alpha = 45°$. It can be found that the variation of the diameter D_0 of the exit channel has a significant effect on the profiles of velocity streamline, pressure, velocity, and shear rate in the spinneret. At a constant mass flow rate W, the variation of diameter D_0 results in different extrusion velocities shown in Figure 11(a,c), which also affects the shear rate in the spinneret shown in Figure 11(d). As shown in Figure 7(c), polymer solution acts like creep flow in the initial region, so there is no much difference in velocity. Afterwards, the velocity profiles start to increase and diverge due to the contraction flow. The overall pressure drop ΔP in the spinneret is also affected greatly by the diameter D_0 of the exit channel, shown in Figure 12. It can be found that the overall pressure drop ΔP decreases dramatically when the diameter D_0 of the exit channel is in the range from 0.15 mm to 0.30 mm. Afterwards, as the diameter D_0 of the exit channel increases, there is little effect on the overall pressure drop ΔP. It also indicates that more deformation energy is dissipated in the spinneret with a smaller diameter.

Figure 13 shows the comparison of profiles of velocity, diameter, temperature, and tensile stress in the air-gap region for the solution extruded from the spinneret with different diameters D_0 of the exit channel under definite $L_s = 0.60$ mm and $\alpha = 45°$. The variation of the diameter D_0 of the exit channel has an obvious effect on the profiles of velocity, diameter, and tensile stress in the air-gap region. As shown in Figure 13(b), for the polymer solution extruded from the exit channel with a small diameter ($D_0 = 0.15$ mm), the diameter of fiber increases in a smooth fashion firstly and then drop gradually. In contrast, for the polymer solution extruded from the exit channel with a large diameter ($D_0 = 0.60$ mm), one observes a fast increase of diameter of fiber and then reduce abruptly till diameter close to the final diameter. The diameter D_0 of the exit channel also influences the die-swell effect shown in Figure 14. As shown in Figure 14, the die-swell ratio B decreases exponentially with the diameter D_0 of the exit channel and could be concluded as following equation: $B = 2.801\exp(-18.182D_0) + 1.446$. The die-swell ratio B firstly reduces sharply with the increase of the diameter D_0 of the exit channel from 0.15 mm to 0.30 mm. Afterwards, as the diameter D_0 of the exit channel increases, the die-swell ratio B decreases slowly. As it is known that the increase of the diameter D_0 of the exit channel leads to the reduction in velocity in the spinneret, which also results in a small shear rate in the spinneret. It is not helpful for polymer chains to generate orientation and stretch in the spinneret. Therefore, little elastic energy of polymers chains has been stored in the spinneret and then lead to a reduction in die-swell phenomena. As shown in Figure 13(d), the tensile stress is nonuniform in the radial direction and the surface tensile stress is always much higher than the centerline tensile stress. For the surface tensile stress, there is a relatively large value when the filament is extruded from the spinneret. For a very small distance beneath the spinneret, there is a drop in surface tensile stress, which due to the sudden change of the boundary conditions from nonslip to free-surface.[36] Afterwards, the surface tensile stress starts to increase at a certain take-up speed. For the centerline tensile stress, it starts to increase gradually when the filament comes out from the spinneret. The tensile stress difference between surface and centerline approaches gradually with the increase of the distance from the spinneret. Another intriguing thing is that the stress difference becomes small with the increase of the diameter D_0 of the exit channel. The uniform tensile stress may result in the uniform microstructure of the filament, ultimately leads to the excellent fiber properties.[37]

CONCLUSIONS

The effect of spinneret geometry, including the entrance angle α of the entrance channel, the length L_s, and the diameter D_0 of the exit channel, on the dynamics of dry-jet wet-spinning of cellulose/[BMIM]Cl solution was predicted by the numerical simulation technology. From the simulated results, the entrance angle α of the entrance channel mainly influences the flow behavior of polymer solution in the spinneret, which also leads to a significant effect on the velocity distribution in the spinneret and die-swell ratio near the spinneret. The decrease of the entrance angle α of the entrance channel could remove the vortices in the corner of the spinneret and reduce die-swell ratio B. However, the variation of the entrance angle α has little effect on the profiles of velocity, diameter, temperature, and tensile stress in the air-gap region. It suggests that a steady flow and an appropriate orientation of polymer solutions in the spinneret could be achieved by optimizing the entrance angle α of the spinneret. The length L_s of the exit channel only affects the pressure drop in the spinneret and die-swell ratio B near the spinneret significantly. By varying the length L_s of the exit channel, the spinability of the polymer solutions could be adjusted by controlling the pressure drop and the die-swell ratio B. Besides, at a constant mass flow rate and draw velocity, the increase of the diameter D_0 of the exit channel is an effective way to reduce the extrusion velocity, pressure drop, and shear rate in the spinneret, resulting in a reduction in the die-swell ratio B as well as tensile stress.

ACKNOWLEDGMENTS

The work is supported by a grant from the National Natural Science Foundation of China (Grant No. 51273041) and Chinese Universities Scientific Fund (CUSF-DH-D-2015018).

REFERENCES

1. Loubinoux, D.; Chaunis, S. *Text. Res. J.* **1987**, *57*, 61.
2. Mortimer, S. A.; Peguy, A. A. *Cell. Chem. Technol.* **1996**, *30*, 117.
3. Fink, H. -P.; Weigel, P.; Purz, H. J.; Ganster, J. *Prog. Polym. Sci.* **1998**, *2*, 387.
4. Swatloski, R. P.; Spear, S. K.; Holbrey, J. D.; Rogers, R. D. *J. Am. Chem. Soc.* **2002**, *124*, 4974.
5. Hermanutz, F.; Meister, F.; Uerdingen, E. *Chem. Fibers. Int.* **2006**, *56*, 342.
6. Hermanutz, F.; Gähr, F.; Uerdingen, E.; Meister, F.; Kosan, B. *Macromol. Symp.* **2008**, *262*, 23.
7. Laus, G.; Bentivoglio, G.; Schottenberger, H.; Kahlenberg, V.; Kopacka, H.; Roder, T.; Sixta, H. *Lenzinger. Berichte* **2005**, *84*, 71.
8. Kosan, B.; Michels, V.; Meister, F. *Cellulose* **2008**, *15*, 59.
9. Cai, T.; Zhang, H. H.; Guo, Q. H.; Shao, H. L.; Hu, X. C. *J. Appl. Polym. Sci.* **2010**, *115*, 1047.
10. Mortimer, S. A.; Peguy, A. A.; Ball, R. C. *Cell. Chem. Technol.* **1996**, *30*, 251.
11. Mortimer, S. A.; Peguy, A. A. *J. Appl. Polym. Sci.* **1990**, *60*, 1747.
12. Kirichenko, A. M.; Kholosha, V. M.; Chemyshow, Y. A.; II'In, V. G.; Nefedova, I. T.; Ambainis, Y. Y. *Fiber. Chem.* **1977**, *8*, 642.
13. Bostwick, C. O. *Text. Res. J.* **1962**, *32*, 819.
14. Pervadchuk, V. P.; Glot, I. O.; Yankov, V. I.; Borisov, A. S.; Vinogradov, Y. A. *Fiber Chem.* **1987**, *18*, 213.
15. Tsebrenko, M. V.; Rezanova, N. M.; Yudin, A. V. *Fiber Chem.* **1980**, *11*, 492.

16. Wang, K. Y.; Matsuura, T.; Chuang, T.-S.; Guo, W. F. *J. Membr. Sci.* **2004**, *240*, 67.
17. Chen, G. Y.; Xu, Y.; Yu, D. G.; Zhang, D. F.; Chatterton, N. P.; White, K. N. *Chem. Commun.* **2015**, *51*, 4623.
18. Zhou, J.; Li, J.; Yu, W.; Li, X.; Zhou, C. *Polym. Eng. Sci.* **2010**, *50*, 1935.
19. Li, Z.; Yuan, X. F.; Haward, S. J.; Odell, J. A.; Yeates, S. *Rheol. Acta* **2011**, *50*, 277.
20. Berry, S. M.; Pabba, S.; Crest, J.; Cambron, S. D.; McKinley, G. H.; Cohn, R. W.; Keynton, R. S. *Polymer* **2011**, *52*, 1654.
21. Xia, X. L.; Yao, Y. B.; Mukuze, K. S.; Zhu, X. J.; Wang, C. S.; Zhang, Y. M.; Wang, H. P. *Mater. Res. Innov.* **2014**, *18*, 874.
22. Xia, X. L.; Gong, M. F.; Wang, C. S.; Wang, B.; Zhang, Y. M.; Wang, H. P. *Cellulose* **2015**, *22*, 1963.
23. Chen, X.; Zhang, Y. M.; Wang, H. P. *J. Rheol.* **2011**, *55*, 485.
24. Chen, X.; Zhang, Y. M.; Cheng, L. Y.; Wang, H. P. *J. Polym. Environ.* **2009**, *17*, 273.
25. Alves, M. A.; Pinho, F. T.; Oliveira, P. J. *AIChE J.* **2005**, *51*, 2908.
26. Boger, D. V. *Annu. Rev. Fluid. Mech.* **1987**, *19*, 157.
27. Walters, K.; Webster, M. F. *Int. J. Numer. Meth. Fl.* **2003**, *43*, 577.
28. Sousa, P. C.; Coelho, P. M.; Oliveira, M. S. N.; Alves, M. A. *Chem. Eng. Sci.* **2011**, *66*, 998.
29. Oliveira, M. S. N.; Oliveira, P. J.; Pinho, F. T.; Alves, M. A. *J. Non-Newton. Fluid Mech.* **2007**, *14*, 92.
30. Aboubacar, M.; Matallah, H.; Webster, M. F. *J. Non-Newton. Fluid Mech.* **2002**, *103*, 65.
31. Alves, M. A.; Poole, R. J. *J. Non-Newton Fluid Mech.* **2007**, *144*, 140.
32. Ansari, M.; Alabbas, A.; Hatzikiriakos, S. G.; Mitsoulis, E. *Int. Polym. Proc.* **2010**, *25*, 287.
33. Liang, J. Z. *Polym. Bull.* **2011**, *67*, 1935.
34. Mu, Y.; Zhao, G. Q.; Zhang, C. R. *J. Appl. Polym. Sci.* **2010**, *117*, 91.
35. Mu, Y.; Zhao, G. Q.; Li, H. P.; Liu, J.; Xu, X. M.; Mu, W. B.; Chen, A. *Polym. Int.* **2009**, *58*, 475.
36. Sun, J.; Subbian, S.; Marchal, J. M. *J. Non-Newton Fluid Mech.* **2000**, *93*, 133.
37. Joo, Y. L.; Sun, J.; Smith, M. D.; Armstrong, R. C.; Brown, R. A.; Ross, R. A. *J. Non-Newton Fluid Mech.* **2002**, *102*, 37.